

Compressive and Tensile Properties of Tungsten-Continuous-Fiber-Reinforced Zr-Based Amorphous Alloy Matrix Composite Fabricated by Liquid Pressing Process

KYUHONG LEE, SANG-BOK LEE, SANG-KWAN LEE, and SUNGHAK LEE

In the present study, a Zr-based amorphous alloy matrix composite reinforced with tungsten continuous fibers was fabricated without pores or defects by a liquid pressing process; the microstructures and mechanical properties of the fibers were investigated. Approximately 60 vol pct of the fibers was distributed inside the amorphous matrix, although the matrix of the composite also contained a small number of polygonal crystalline phases. The tensile strength of the composite was about 30 pct higher than that of the amorphous alloy, because of the very strong reinforcement of the tungsten fibers and because of the strong fiber/matrix interfacial bonding. The shear fracture of the amorphous matrix was significantly constrained by the fibers, and fracture proceeded almost perpendicular to the tensile direction. According to the compressive test results of the composite, fracture did not take place as a one-time occurrence after the maximum strength point, but proceeded as the loading was sustained by the fibers, thereby leading to a maximum strength of 2477 MPa and a plastic strain of 1.5 pct. The fibers played an important role in improving the ductility, by interrupting the propagation of shear cracks initiated at the amorphous matrix and by taking over a considerable number of compressive loads in the area in which the cracks were formed, while the fibers themselves were buckled. These findings suggested that the liquid pressing process was useful for the development of amorphous matrix composites with improved mechanical properties.

DOI: 10.1007/s11661-008-9528-z

© The Minerals, Metals & Materials Society and ASM International 2008

I. INTRODUCTION

REMARKABLE advances in amorphous alloys have been made because amorphous alloys with high glass-forming ability have been developed by conventional casting methods.^[1-5] Among these alloys, Zr-based amorphous alloys, in particular, possess a very high glass-forming ability (critical cooling rate: about 1 °C/s; maximum sample diameter: 50 to approximately 60 mm), together with high hardness, stiffness, strength, and corrosion resistance,^[1,3] and thus have been used in high-performance structural components such as electronic parts, sporting goods, and defense industry parts. However, Zr-based amorphous alloys have poor ductility because brittle fracture readily occurs, due to the formation of localized shear bands under tensile or compressive loading condition,^[6,7] thereby limiting wide application in advanced structural materials. Thus, if

the fabrication of amorphous alloy matrix composites, in which secondary phases or reinforcements are homogeneously dispersed in the amorphous alloy matrix, can be newly developed, the aforementioned problems of amorphous alloys can be solved while their advantages are retained. Methods of fabricating amorphous matrix composites include the addition of crystalline particles to the amorphous melt,^[8,9] the casting of both reinforcing fibers and amorphous alloys,^[10,11] the generation of dendritic crystalline phases from the amorphous melt,^[12] and the partial crystallization of amorphous alloys to disperse nanocrystallines.^[13,14]

In order to effectively fabricate amorphous matrix composites reinforced with metallic continuous fibers, it is necessary to introduce new-concept fabrication technologies, one of which is a liquid pressing process.^[15] Because this process uses low pressure—nearly the theoretically required minimum loading pressure, in fact—the crystallization of the amorphous matrix can be prevented or minimized by the rapid cooling of the amorphous melt. This process also has the advantage of complete infiltration of the melt inside the fiber preform, due to the application of low hydrostatic pressure and the elimination of the pores formed by contraction during solidification. This process can also be used in the fabrication of large-scale amorphous composites reinforced with two- or three-dimensional fibers as well as with one-dimensional continuous fibers.

In this study, tungsten continuous fibers that have high strength and thermal stability were used for

KYUHONG LEE, Postdoctoral Research Associate, is with the Center for Advanced Aerospace Materials, Pohang University of Science and Technology, Pohang, 790-784, Korea. SUNGHAK LEE, Professor, Center for Advanced Aerospace Materials, is jointly appointed with Materials Science and Engineering, Pohang University of Science and Technology. Contact email: shlee@postech.ac.kr SANG-BOK LEE and SANG-KWAN LEE, Senior Researchers, are with the Composite Materials Laboratory, Korea Institute of Materials Science, Changwon, 641-010, Korea.

Manuscript submitted December 14, 2007.

Article published online April 16, 2008

reinforcements. An amorphous matrix composite, the matrix of which was a Zr-based amorphous alloy, was fabricated by the liquid pressing process. Microstructures of the fabricated composite were analyzed and its mechanical properties were evaluated by conducting tensile and compressive tests. Deformation and fracture mechanisms were analyzed by observing the fracture surfaces and deformed areas of the fractured composite specimens under tensile and compressive loading conditions.

II. EXPERIMENTAL

The Zr-base amorphous alloy used for the composite matrix was an “LM1” alloy, which is a commercial brand name of the Liquidmetal Technologies (Lake Forest, CA). Its chemical composition is $Zr_{41.2}Ti_{13.8}Cu_{12.5}Ni_{10.0}Be_{22.5}$ (atomic percent), and it has very high amorphous forming ability, hardness, strength, and corrosion resistance.^[1,16] Tungsten continuous fibers with a high melting temperature, strength, and thermal stability inside the melted matrix were used as reinforcements. A scanning electron micrograph of tungsten fibers and an optical micrograph of the Zr-based amorphous (LM1) alloy are shown in Figures 1(a) and (b), respectively. The diameter of the tungsten fibers is about $100\ \mu\text{m}$ (Figure 1(a)), and the surface of the fibers is somewhat rough (average surface roughness, R_a : $1.2\ \mu\text{m}$). In the LM1 alloy, fine polygonal crystalline particles 2 to approximately $3\ \mu\text{m}$ in size are distributed in the amorphous matrix (Figure 1(b)). These crystalline particles are identified as fcc phases^[17] (lattice parameter: $1.185\ \text{nm}$), and their volume fraction is 1.9 pct. The representative physical properties of the LM1 alloy and tungsten fibers are summarized in Table I.

A schematic diagram of the liquid pressing process^[15] used to fabricate the Zr-based amorphous matrix composite is shown in Figure 2. The size of the mold interior is $60 \times 60 \times 6\ \text{mm}$. A preform of tungsten fibers and LM1 alloy plates was inserted into the mold, and was degassed and vacuumed. The mold was heated to $870\ ^\circ\text{C}$, held for 5 minutes, and then pressed under a pressure of about 10 MPa. Pressing was accompanied by water cooling, so that the solidified matrix could readily form amorphous phases.

The composite was sectioned, polished, and etched in a solution of 70 mL of H_2O , 25 g of CrO_3 , 20 mL of HNO_3 , and 2 mL of HF , for optical and scanning electron microscope (SEM) observations. The volume fractions of tungsten fiber and polygonal crystalline particles in the matrix were measured by an image analyzer. The phases formed in the composite were analyzed by transmission electron microscopy (TEM). For the TEM observation, specimens were mechanically polished to a thickness of $100\ \mu\text{m}$, and were punched to prepare disk specimens (diameter: 3 mm) using a disk cutter. Disks were further thinned by dimpling to a minimum thickness of 40 to approximately $50\ \mu\text{m}$, and ion milled to prepare thin foils. The thin foils were observed by a transmission electron

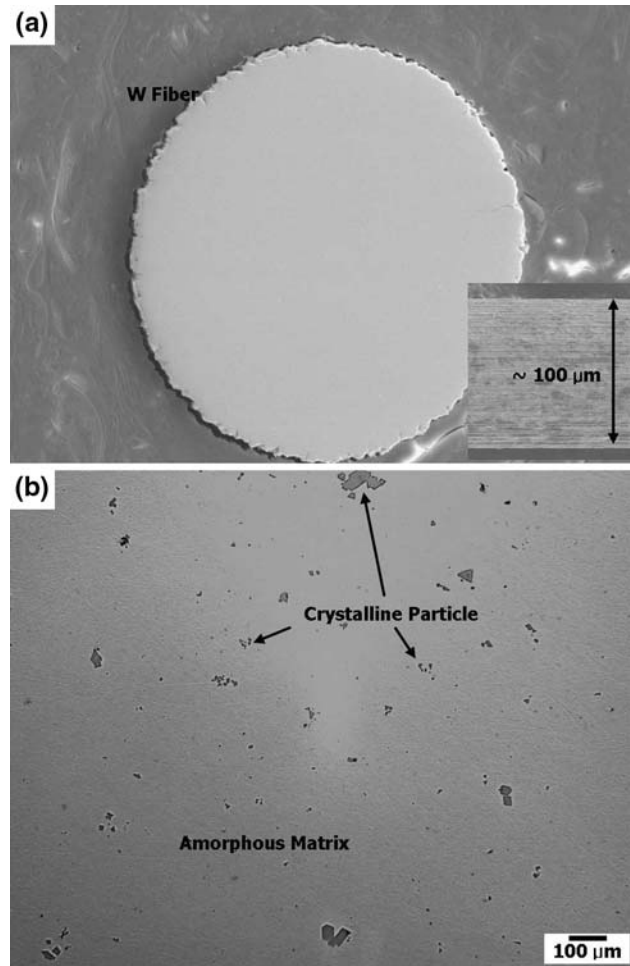


Fig. 1—(a) SEM micrograph of tungsten continuous fibers and (b) optical micrograph of Zr-based amorphous (LM1) alloy.

microscope (model JEM-2100F, JEOL*) operating at

*JEOL is a trademark of Japan Electron Optics Ltd., Tokyo.

an acceleration voltage of 200 kV. The amorphous forming properties of the LM1 matrix alloy and composite were analyzed by a differential scanning calorimeter (DSC) (model DSC-7, Perkin-Elmer, Waltham, MA) at a heating rate of $20\ ^\circ\text{C}/\text{min}$.

The composite was machined into rectangular bar specimens $2 \times 2 \times 3\ \text{mm}$ in size, and room-temperature compression tests were conducted on these specimens at a crosshead speed of 1 mm/min. Plate-type tensile specimens with a gage length of 5 mm, a width of 2 mm, and a thickness of 2 mm were prepared, and were tested at room temperature at a crosshead speed of 0.1 mm/min. Tensile and compressive testing was performed by a universal testing machine (model 5567, Instron, Norwood, MA) with a capacity of 3000 kg. Fractured specimens were observed by an SEM after the tests. Tensile tests of tungsten continuous fibers (length: 150 mm) were also performed using a small-scale universal testing machine (model 1453, Zwick, Ulm,

Table I. Physical and Mechanical Properties of Tungsten Fibers and Zr-Based Amorphous Alloy (LM1 Alloy)

Material	Diameter (μm)	Density (g/cm^3)	Thermal Expansion Coefficient ($10^{-6}/^\circ\text{C}$)	Melting Temperature ($^\circ\text{C}$)	Elastic Modulus (GPa)
Tungsten fiber	~100	19.3	4.6	3370	411
LM1 alloy	—	6.1	8.5	720	97

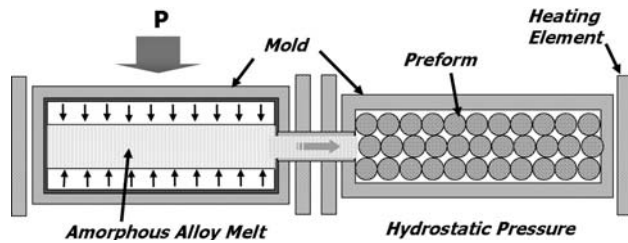


Fig. 2—Schematic diagram of liquid pressing process.

Germany) with capacity of 500 kg at a crosshead speed of 100 mm/min. Three-point bending tests were also conducted, to evaluate the flexural bonding strength of the fiber/matrix interfaces. Test specimens $3.5 \times 6.5 \times 23$ mm in size were tested at a crosshead speed of 1 mm/min at room temperature using a universal testing machine (model 5882, Instron), in accordance with the ASTM E855 specification.^[18] Each mechanical test was conducted at least five times and the data were averaged.

III. RESULTS

A. Microstructure

Figure 3 shows the DSC curves of the LM1 alloy and tungsten-fiber-reinforced composite. The glass transition temperatures (T_g) of the alloy and composite are similar at 364°C and 358°C , respectively. This implies that properties of the amorphous matrix are only minimally changed during the liquid pressing process. The crystallization temperatures (T_x) of the composite is 399°C , which is lower by 33°C than that of the LM1

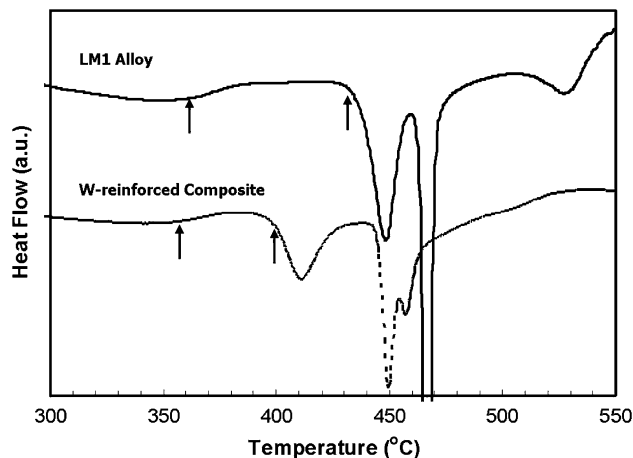


Fig. 3—DSC curves of Zr-based amorphous alloy and tungsten-fiber-reinforced amorphous matrix composite.

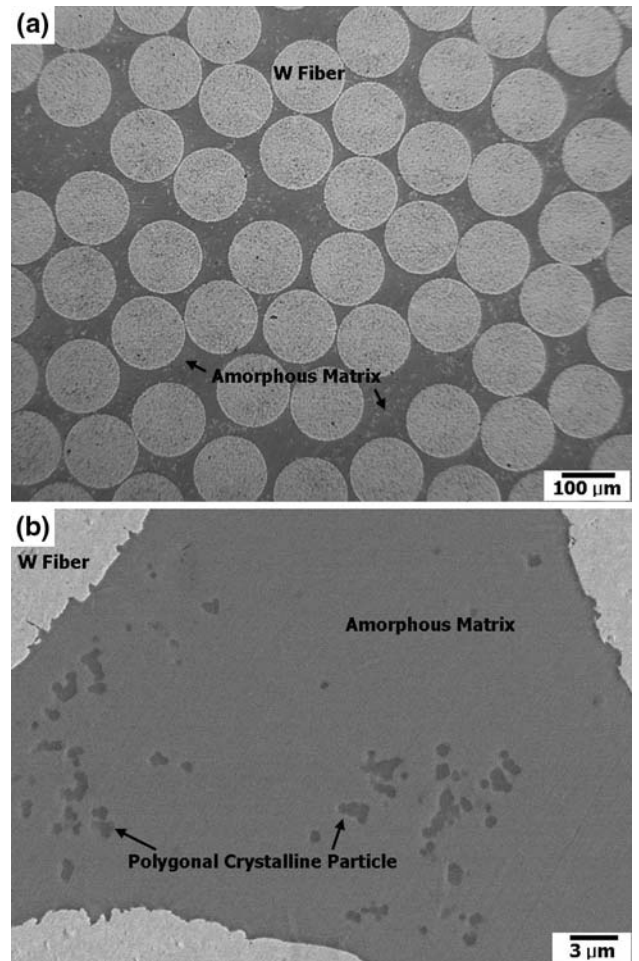


Fig. 4—(a) Optical and (b) SEM micrographs of tungsten-fiber-reinforced amorphous matrix composite.

alloy (432°C). This is because the crystallization of the amorphous matrix occurs at a lower temperature, because the surface of the tungsten fibers acts as the initiation sites for crystallization.

Figures 4(a) and (b) are optical and SEM micrographs of the tungsten-fiber-reinforced composite. Tungsten fibers are distributed in the matrix, and their volume fraction is 60.8 pct, as analyzed from the cross-sectional micrograph of the composite (Figure 4(a)). In the matrix, fine polygonal crystalline particles are observed (Figure 4(b)); their fraction is measured to be 2.2 pct, which is similar to that in the LM1 alloy (Figure 1(b)). Only a minimal number of pores or defects formed by misinfiltration, or reaction products formed by the interfacial reaction at the fiber/matrix interfaces, are found. This indicates the successful

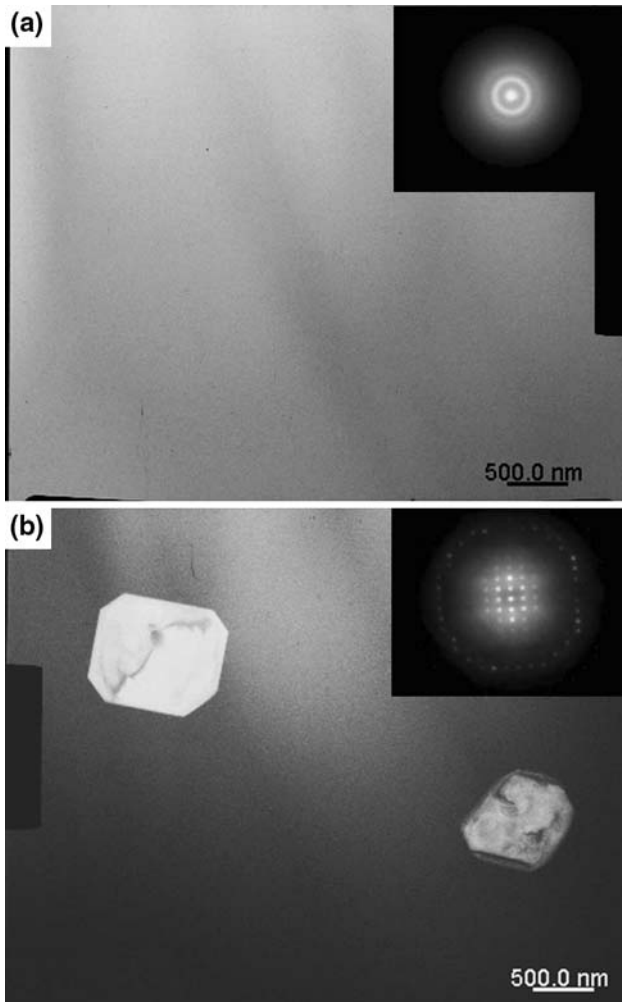


Fig. 5—TEM bright-field images of the (a) matrix and (b) polygonal crystalline particles of the tungsten-fiber-reinforced composite. Insets in (a) and (b) show diffraction patterns of amorphous matrix and polygonal crystalline particles.

fabrication of the amorphous matrix composite by the liquid pressing process.

Figures 5(a) and (b) are TEM bright image and diffraction patterns obtained from the composite matrix and fiber/matrix interface. The matrix consists of amorphous phases together with a small number of polygonal crystalline particles, as shown in Figures 5(a) and (b). The amorphous phases show diffused ring patterns, which are typical in amorphous alloys, without spots (Figure 5(a)). Figure 5(b) shows fcc crystalline particles and their diffraction pattern in the [114] zone axis. The lattice parameter of polygonal crystalline particles is calculated to be 12.05 Å, thereby implying that these particles are almost identical to the polygonal particles present in the LM1 alloy of Figure 1(b).

B. Tensile Properties of Tungsten-Fiber-Reinforced Composite

Figures 6(a) and (b) present the tensile and compressive stress-strain curves of the LM1 alloy and tungsten-fiber-reinforced composite; Table II summarizes the

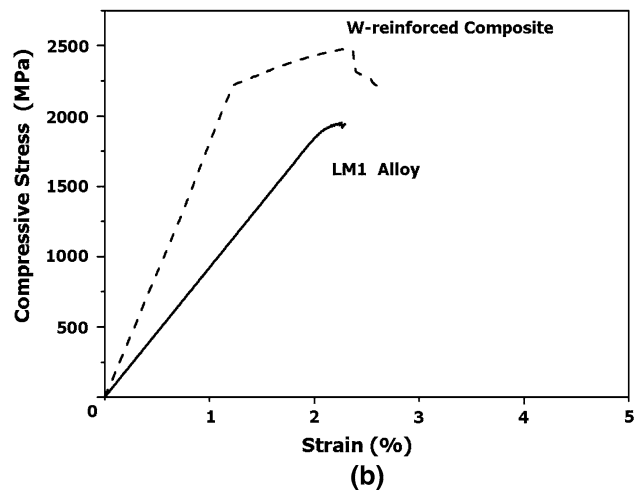
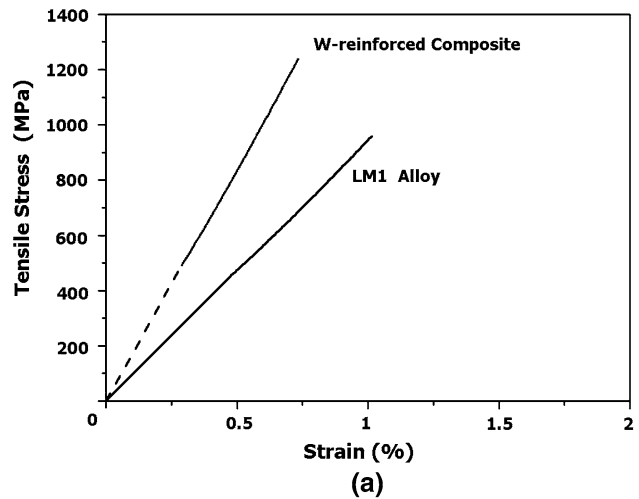


Fig. 6—(a) Tensile and (b) compressive stress-strain curves of the LM1 alloy and tungsten-fiber-reinforced composite.

tensile and compressive test results together with the tensile test results of the tungsten fibers. The tensile strength of the LM1 alloy is 956 MPa, which is about half the strength under compressive loading, and the ductility is almost nil. It is generally reported that very fine pores and crystalline phases are present inside cast amorphous alloys.^[19,20] These pores and crystalline phases readily develop into voids or cracks under tensile loading and lead to fracture at a stress lower than the maximum compressive strength, whereas they only minimally affect the compressive properties.^[21] The tensile strength of the composite is 1239 MPa, which is about 30 pct higher than that of the LM1 alloy, but the tensile elongation is only minimally present, similar to the LM1 alloy. The increase in the tensile strength is associated with the containment of high-strength tungsten fibers.

Figures 7(a) through (c) show SEM micrographs of the side region and a fractograph of the tensile test specimen of the composite. The fracture surface is perpendicular to the tensile direction, in general, and fiber pullouts are only minimally observed (Figure 7(a)). This implies a very strong fiber/matrix interfacial

Table II. Compressive and Tensile Test Results of the Zr-Based Amorphous Alloy (LM1 Alloy), Tungsten Fibers, and Tungsten-Fiber-Reinforced Amorphous Matrix Composite

Material	Loading Mode	Yield Strength (MPa)	Ultimate Strength (MPa)	Total Strain (Pct)	Plastic Strain (Pct)
LM1 alloy	compressive	1920	1943	2.2	0.2
	tensile	956	956	~1	~0
Tungsten fiber	tensile	2395	2395	~1	~0
Tungsten-fiber-reinforced composite	compressive	2258	2477	2.6	1.5
	tensile	1239	1239	~1	~0

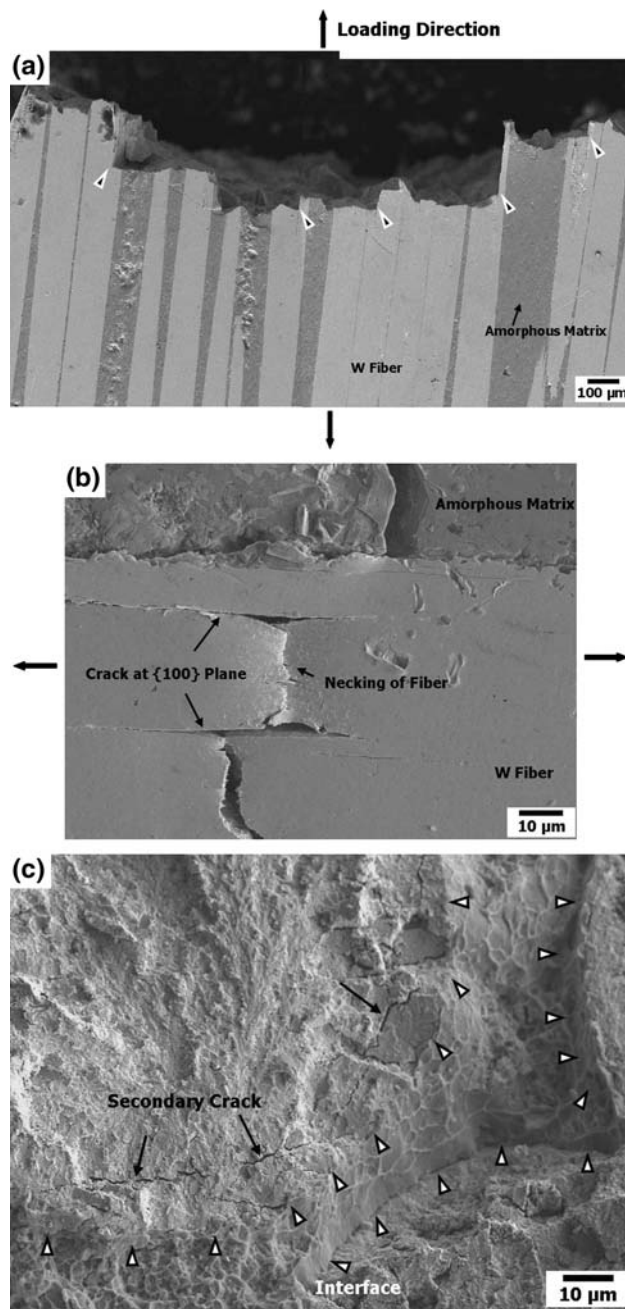


Fig. 7—(a) and (b) SEM micrographs of the side region and (c) SEM fractograph of the tensile test specimen of the tungsten-fiber-reinforced composite.

bonding. Inside the tungsten fibers, longitudinal cracks parallel to the tensile axis are often observed, as indicated by white arrows. Some fibers beneath the fracture surface are longitudinally cracked, and necking can occur between these cracks, as shown in Figure 7(b). The fracture surface consists of vein patterns in the matrix region and cleavage facets in the tungsten fiber region (Figure 7(c)). Fiber/matrix interfaces are visible, and secondary cracks are shown inside the tungsten fibers, as marked by the arrows.

C. Compressive Properties of Tungsten-Fiber-Reinforced Composite

Figure 6(b) shows compressive stress-strain curves of the LM1 alloy and composite; their yield compressive strength, maximum compressive strength, and elongation are summarized in Table II. The yield and maximum compressive strengths of the LM1 alloy are 1920 and 1943 MPa, respectively, and the elongation is approximately 2 pct. The maximum strength of the composite is 2258 MPa, which is about 30 pct higher than that of the LM1 alloy. The composite shows the yielding phenomenon, and its plastic strain is about 1.5 pct. Fracture does not take place as a one-time occurrence after reaching the maximum strength, but proceeds as the compressive load is sustained by fibers.

Figures 8(a) and (b) show the SEM micrograph of the side region and the fractograph, respectively, of the compressively fractured specimen of the composite. Fracture proceeds at the maximum shear stress direction (at an approximately 45-deg angle to the compressive loading direction) as in typical amorphous alloys, but there remain some connected fibers that are not cut off (Figure 8(a)). This shows that the amorphous matrix undergoes slow cracking and fracture, instead of abrupt fracture at one time, because fibers work to withstand the applied load, even after reaching the maximum strength, thereby showing a considerable amount of ductility. Longitudinal cracks along the compressive loading direction are observed inside the fibers, and some fibers are buckled while they sustain the loading. Cracks initiate along the maximum shear stress direction in the matrix, but the crack propagation is interrupted by fibers. Here, the fiber/matrix interfacial separation is hardly found. The fracture surface contains vein patterns in the matrix region and cleavage facets of the tungsten fibers (Figure 8(b)).

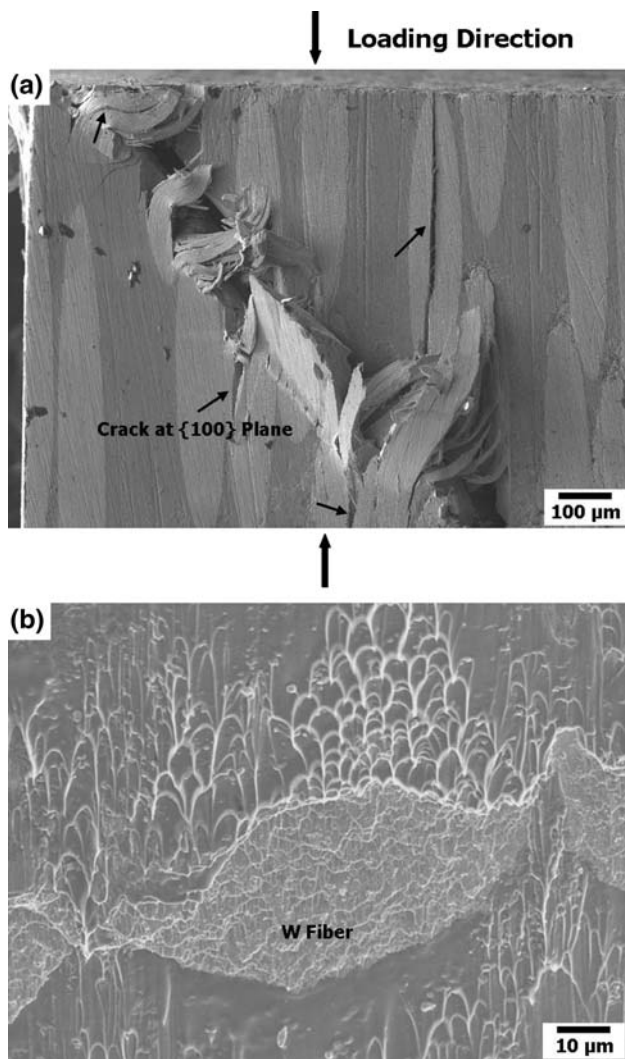


Fig. 8—(a) SEM micrograph of the side region and (b) SEM fractograph of the compressive test specimen of the tungsten-fiber-reinforced composite.

IV. DISCUSSION

A. Fabrication of Tungsten-Fiber-Reinforced Amorphous Matrix Composite by Liquid Pressing Process

Because the hydrostatically applied pressure in the liquid pressing process of this study readily overrides the theoretical pressure required for infiltration, the amorphous melt sufficiently infiltrates into the fiber preform, and pores formed by solidification or contraction are eliminated. Crystalline phases other than the polygonal crystalline particles are not found in the amorphous matrix (Figure 4(b)), which indicates that the crystallization due to the diffusion from the tungsten fibers to the matrix or due to the fiber/matrix interfacial reaction did not occur during the liquid pressing process. This is because of the high thermal stability of tungsten fibers; the melting temperature of tungsten fibers is 3370 °C, which is much higher than the maximum processing temperature (870 °C). This also implies a successful fabrication of the tungsten-fiber-reinforced amorphous matrix composite by the liquid pressing process.

The tensile strength of the tungsten-fiber-reinforced composite was calculated by the rule of mixtures. The calculated tensile strength is 1819 MPa, which is 580 MPa higher than the measured tensile strength (1239 MPa). The reasons behind the higher calculated strength of the composite include: (1) the residual tensile stress acts as a buffer of the tensile stress during the tensile test^[22] and (2) tungsten fibers can be cracked at a stress lower than the calculated stress, because of the stress concentration. According to a previous study^[23] of the tungsten-fiber-reinforced amorphous matrix composite, the tensile residual stress of approximately 100 MPa was present in the matrix along the longitudinal direction of the fibers. This is useful for initiating the fracture at a strength lower than the tensile strength of the matrix during the tensile test. In addition, the fibers might be readily fractured, because cracks or shear bands formed at the amorphous matrix cause the stress concentration at the tungsten fiber/matrix interfaces. These reasons might make the composite fracture at a tensile stress lower than the stress calculated by the rule of mixtures. The compressive strength of the composite could not be calculated by the rule of mixtures, because the compressive strength of tungsten fibers could not be obtained.

In general, fiber-reinforced composites have properties that differ according to the fiber arrangement directions or loading directions, because of the brittle fiber/matrix interfaces. In order to investigate the fiber/matrix interfacial bonding strength, the three-point bend test was conducted, and a bending shear stress-displacement curve and an SEM micrograph of the side region of the specimen are shown in Figures 9(a) and (b), respectively. The maximum bending shear strength measured from the curve is 131 MPa (Figure 9(a)). During the test, the specimen is subjected to tensile, shear, and compressive stresses, depending on the specimen location. Figure 9(b) shows that fiber pullout or interfacial separation is only minimally observed, irrespective of loading conditions, thereby indicating quite a strong fiber/matrix interfacial bonding.

B. Fracture Mechanisms of Tungsten-Fiber-Reinforced Amorphous Matrix Composite under Compressive and Tensile Loading Conditions

Amorphous alloys only minimally show plastic regions under tensile or compressive loading conditions, because plastic deformation is generally concentrated on one or two shear bands at room temperature.^[6,7] This localized plastic deformation at shear bands is very large, and only one or two shear bands lead to final brittle fracture. In the tungsten-fiber-reinforced composite fabricated in the present study, however, fibers favorably affect the strength and ductility through various mechanisms, such as inhibition of the shear crack propagation initiated from the amorphous matrix and fiber buckling under compressive loading; the plastic deformation only minimally occurs, however, as in the LM1 alloy, under tensile loading.

The tensile strength of the composite improves by about 30 pct because the reinforcement of tungsten fibers have a strength higher than that of the LM1 alloy.

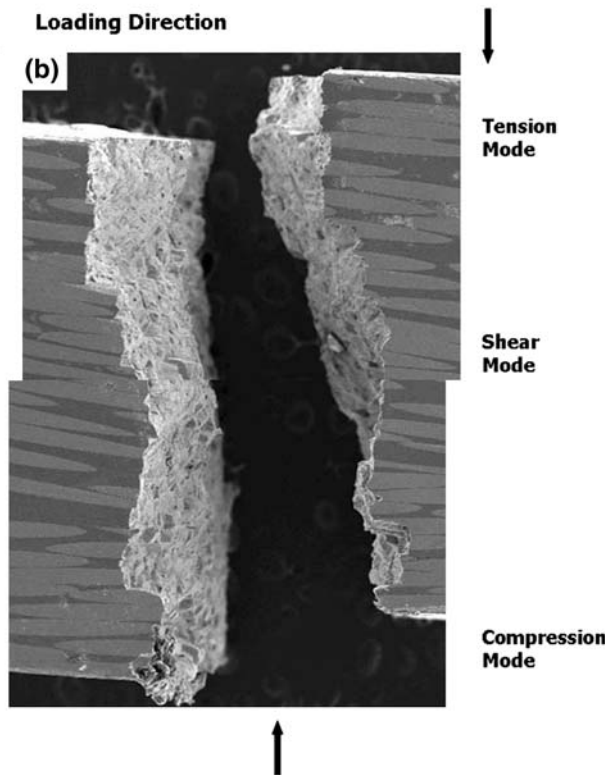
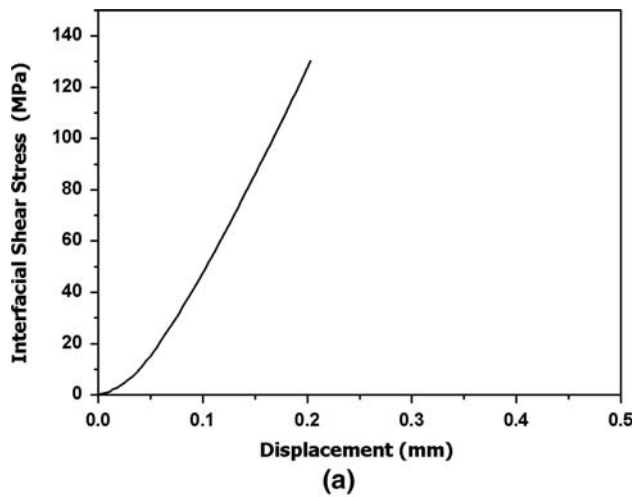


Fig. 9—(a) Bending shear stress-displacement curve and (b) SEM micrograph of the side region of the bending test specimen of the tungsten-fiber-reinforced composite.

Tungsten fibers do not contribute to the improvement of the tensile ductility of the composite, because they only minimally show the tensile elongation, as indicated in Table II. However, shear fracture of the amorphous matrix is significantly constrained by the fibers, and fracture proceeds almost perpendicular to the tensile direction, as shown in Figure 7(a). Cracks initiated from the amorphous matrix propagate into the tungsten fibers, but often change their path abruptly at an almost 90-deg angle inside the fibers, thereby showing the stair-type propagation path (arrows in Figure 7(a)). This is because the cleavage planes of the tungsten fibers, which have a bcc structure, are $\{100\}$ planes that consume the

least plastic energy at the crack initiation.^[24] Kim *et al.*^[25] investigated the crack initiation and propagation behavior of tungsten particles by *in-situ* SEM fracture tests of tungsten heavy alloys, and observed the formation of cleavage facets at almost 90 deg to each other. Inside the tungsten fibers of the present composite, cracks are often formed at about 90 deg, and are observable as secondary cracks on tensile fracture surfaces (Figure 7(c)). The fracture surfaces are composed of vein patterns of the amorphous matrix region and cleavage facets of the fiber region, and secondary cracks are found inside the fiber region. Thus, the tungsten fibers interrupt the rapid propagation of cracks initiated from the amorphous matrix and take over loads applied to the cracked matrix areas; this improves the strength of the composite.

The plastic strain of the LM1 alloy is almost nil under compressive loading, but the tungsten-fiber-reinforced composite shows a plastic strain of 1.5 pct. This is because tungsten fibers show some plastic deformation, such as buckling, and work to withstand a considerable number of applied compressive loads, while the amorphous matrix is fractured by shear cracking (Figure 8(a)). As shown in the compressive stress-strain curve of Figure 6(b), the compressive stress maintains 2200 to approximately 2300 MPa after the maximum compressive stress point, through the plastic deformation of fibers. This stress-strain behavior is associated with the strong fiber/matrix interfaces. Inside the tungsten fibers, some longitudinal cracks are formed along the compressive loading direction (Figure 8(a)). These cracks lie on $\{100\}$ planes of tungsten fibers, and play a role in interrupting the propagation of shear cracks initiated at the amorphous matrix occurring at 50- to approximately 60-deg angles to the compressive loading direction. Thus, during the compressive test of the composite, the fibers play an important role in improving the ductility, by interrupting the radical propagation of the shear cracks initiated at the amorphous matrix and by taking over a considerable number of compressive loads, while the fibers themselves are buckled. In addition, the strong fiber/matrix bonding strength and the increased elongation improve the compressive strength of the composite over the LM1 alloy by about 27 pct.

It is interesting to note that the size of the vein patterns formed in the amorphous matrix decreases as the vein patterns reach the tungsten fibers (that is, as the distance between the vein patterns and the tungsten fibers decreases) (Figure 8(b)). In the LM1 alloy, the fracture surfaces generally show vein patterns, as shear band planes are locally melted by the heat generated during deformation.^[26,27] Large vein patterns imply the fast propagation speed of shear bands, as a considerable amount of plastic flow exists before local melting and solidification, whereas small vein patterns indicate the slow propagation speed of shear bands.^[28] The decrease in the vein pattern size indicates the interruption of the abrupt shear band propagation in the amorphous matrix by the fibers, which confirms the role of tungsten fibers in interrupting the shear band propagation.

Based on the findings of this study of tungsten-fiber-reinforced amorphous matrix composite fabricated by

the liquid pressing process, the fabrication process of the composite is well understood, and the fact that the strength and ductility of the LM1 alloy can be improved while the advantages of the LM1 alloy are retained. Using the liquid pressing process, the composite with strong fiber/matrix bonding can be successfully fabricated without defects such as pores and misinfiltration. Because this composite possesses enhanced properties of strength and ductility, it presents new possibilities that can be applied to structural materials that require excellent properties. The fracture toughness of the composite might be improved, because the propagation of shear bands or cracks initiated at the amorphous matrix can be effectively interrupted by tungsten fibers. In order to further enhance the microstructure and properties of continuous-fiber-reinforced amorphous matrix composites, more intensive studies should be completed; these studies would aim to select new fibers and matrix alloys, establish optimized liquid pressing conditions, and clarify mechanisms involved in improved strength, ductility, and fracture toughness.

V. CONCLUSIONS

In the present study, the tungsten-continuous-fiber-reinforced Zr-based amorphous matrix composite was fabricated by a liquid pressing process, and its microstructures and compressive and tensile properties were investigated, with the following results.

1. The composite with strong fiber/matrix interfaces was successfully fabricated without pores and misinfiltration through the liquid pressing of tungsten fibers and a Zr-based amorphous alloy. About 60 vol pct of the fibers was distributed in the matrix, in which a small amount of polygonal crystalline particles were present.
2. The tensile strength of the composite was about 30 pct higher than that of the amorphous alloy, because of the high-strength reinforcement of the tungsten fibers. The shear fracture of the amorphous matrix was significantly constrained by fibers, and fracture proceeded almost perpendicular to the tensile direction. The tensile fracture surface of the composite was composed of vein patterns of the amorphous matrix and cleavage facets of the tungsten fibers; secondary cracks were found inside fiber areas.
3. According to the compressive test results of the composite, fracture did not take place in a one-time occurrence after the maximum strength point, but proceeded as the loading was sustained by fibers, thereby leading to the maximum strength of 2477 MPa and the plastic strain of 1.5 pct. Fibers played an important role in improving the ductility, by interrupting the radical propagation of shear cracks initiated at the amorphous matrix and by taking over a considerable number of compressive loads in the area in which the cracks were formed, while the fibers themselves were buckled.

ACKNOWLEDGMENTS

This work was supported by the fundamental research funds of the Korea Institute of Materials Science (Changwon, Korea), "Development of Amorphous Matrix Composites Reinforced with Ductile Metallic Fiber," and by the National Research Laboratory Program (Grant No. M10400000361-06J0000-36110), funded by the Korea Science and Engineering Foundation.

REFERENCES

1. A. Peker and W.L. Johnson: *Appl. Phys. Lett.*, 1993, vol. 63, pp. 2342–44.
2. A. Inoue, N. Nishiyama, and T. Matsuda: *Mater. Trans., JIM*, 1996, vol. 37, pp. 181–84.
3. A. Inoue, T. Zhang, N. Nishiyama, K. Ohba, and T. Masumoto: *Mater. Trans., JIM*, 1993, vol. 34, pp. 1234–37.
4. K.H. Kim, S.W. Lee, J.P. Ahn, E. Fleury, Y.C. Kim, and J.C. Lee: *Met. Mater. Int.*, 2007, vol. 13, pp. 21–24.
5. A. Inoue, T. Zhang, and A. Takenchi: *Appl. Phys. Lett.*, 1997, vol. 71, pp. 464–66.
6. H.A. Bruck, T. Christman, and W.L. Johnson: *Scripta Metall.*, 1994, vol. 30, pp. 429–34.
7. Y. Kawamura, T. Shibata, A. Inoue, and T. Masumoto: *Appl. Phys. Lett.*, 1996, vol. 69, pp. 1208–10.
8. H. Choi-Yim and W.L. Johnson: *Appl. Phys. Lett.*, 1997, vol. 71, pp. 3808–10.
9. D.H. Bae, H.K. Lim, S.H. Kim, D.H. Kim, and W.T. Kim: *Acta Mater.*, 2002, vol. 50, pp. 1749–59.
10. R.D. Conner, R.B. Dandliker, and W.L. Johnson: *Acta Mater.*, 1998, vol. 46, pp. 6089–6102.
11. P. Wadhwa, J. Heinrich, and R. Busch: *Scripta Mater.*, 2006, vol. 56, pp. 73–76.
12. C.C. Hays, C.P. Kim, and W.L. Johnson: *Phys. Rev. Lett.*, 2000, vol. 84, pp. 2901–04.
13. C.M. Lee, S.W. Chae, H.J. Kim, and J.C. Lee: *Met. Mater. Int.*, 2007, vol. 13, pp. 191–96.
14. C. Fan and A. Inoue: *Mater. Trans., JIM*, 1999, vol. 40, pp. 42–51.
15. Y.H. Jang, S.S. Kim, Y.C. Jung, and S.K. Lee: *J. Kor. Inst. Met. Mater.*, 2004, vol. 42, pp. 425–31.
16. W.H. Wang, C. Dong, and C.H. Shek: *Mater. Sci. Eng., R*, 2004, vol. R44, pp. 45–89.
17. Q. Wei, N. Wanderka, P. Schubert-Bischoff, M.-P. Macht, and S. Friedrich: *J. Mater. Res.*, 2000, vol. 15, pp. 1729–34.
18. *ASTM Standard Test Method for Bend Testing of Metallic Flat Materials for Spring Applications Involving Static Loading*, ASTM E855-90, ASTM, Philadelphia, PA, 2000.
19. J.G. Lee, D.G. Lee, S. Lee, K.M. Cho, I. Park, and N.J. Kim: *Mater. Sci. Eng., A*, 2005, vol. A390, pp. 427–36.
20. G.B. Cho, Y.H. Kim, S.G. Hur, C.A. Yu, and T.H. Nam: *Met. Mater. Int.*, 2006, vol. 12, pp. 173–79.
21. M.L. Lee, Y. Li, and C.A. Schuh: *Acta Mater.*, 2004, vol. 52, pp. 4121–31.
22. R.J. Arsenault and M. Taya: *Acta Metall.*, 1987, vol. 35, pp. 651–59.
23. S.B. Lee, J.B. Kim, S.K. Lee, S. Lee, and N.J. Kim: *J. Kor. Inst. Met. Mater.*, 2006, vol. 44, pp. 794–800.
24. R. Ayres and D.F. Stein: *Acta Metall.*, 1971, vol. 19, pp. 789–94.
25. D.K. Kim, S. Lee, and H.S. Song: *Metall. Mater. Trans. A*, 1999, vol. 30A, pp. 1261–73.
26. L.Q. Xing, J. Eckert, and L. Schultz: *Nanostruct. Mater.*, 1999, vol. 12, pp. 503–06.
27. N.T. Nhan, P.K. Hung, D.M. Nghiep, T.Q. Thang, and H.S. Kim: *Met. Mater. Int.*, 2006, vol. 12, pp. 167–72.
28. H. Choi-Yim, R. Busch, U. Koster, and W.L. Johnson: *Acta Mater.*, 1990, vol. 47, pp. 2455–62.